

# Canted antiferromagnetism in high purity $\text{NaFeF}_3$ prepared by a novel wet-chemical synthesis method

Fabian L. M. Bernal, Bruno Gonano, Fredrik Lundvall, David S. Wragg, and Helmer Fjellvåg  
*Chemistry Department and Center for Material Science and Nanotechnology, University of Oslo, NO-0315, Oslo, Norway*

Fabien Veillon  
*Laboratory Crismat, UMR6508 CNRS, Normandie University,  
 ENSICAEN, UNICAEN, 6 bd Maréchal Juin, 1450 Caen cedex 4, France*

Wojciech A. Sławiński  
*Faculty of Chemistry, University of Warsaw, Pasteura 1, 02-093 Warsaw, Poland and  
 ISIS Facility, Rutherford Appleton Laboratory, Harwell Oxford, Didcot, Oxfordshire OX11 0QX, U.K.*

Øystein S. Fjellvåg  
*Department for Neutron Materials Characterization,  
 Institute for Energy Technology, PO Box 40, NO-2027, Kjeller, Norway*

We report a novel synthesis method for, and structural and magnetic characterization of the fluoroperovskite  $\text{NaFeF}_3$ . We have developed a wet-chemical method that allows preparation of large volumes of air-sensitive fluoroperovskites with high purity.  $\text{NaFeF}_3$  has a Néel temperature ( $T_N$ ) of 90 K and a Weiss constant ( $\theta$ ) of -124 K, corresponding to dominant antiferromagnetic interactions. Below  $T_N$ , a slight difference is observed between zero-field and field cooled samples, indicating spin-canting and weak ferromagnetism. AC magnetometry confirms that weak ferromagnetism is inherent to  $\text{NaFeF}_3$  and not due to impurities. From powder neutron diffraction data, we describe the magnetic structure precisely as a weakly canted G-type (magnetic space group  $Pn'ma'$ ). A ferromagnetic component is allowed in  $Pn'ma'$ , however, this component may be absent in zero magnetic fields and is too small to be confirmed on the basis of powder neutron diffraction data.

## I. INTRODUCTION

Fluoroperovskites display rich structural chemistry, strongly ionic bonding character (due to the high electronegativity of the fluoride anions), and corresponding localized electron magnetism [1, 2]. They exhibit a wide range of properties that can be utilized in e.g. data storage, computer processors, spintronics, multiferroics and batteries [3–6].

$\text{NaFeF}_3$  has attracted attention as a low-cost cathode material [7, 8]. Its advantages in this application include the Earth's abundance of the constituent elements, intrinsic anion stability and a theoretical capacity of 197  $\text{mAhg}^{-1}$  for a one-electron process.  $\text{NaFeF}_3$  nanoplates in particular show good capacity retention compared to other metal fluoride and composite cathode materials with 50% retained capacity for Na after 200 cycles at 0.2  $\text{A g}^{-1}$  [9].

The  $\text{NaFeF}_3$  fluoroperovskite has intriguing phase relations under high-pressure. At ambient temperature and pressure, the compound adopts the orthorhombic perovskite  $\text{GdFeO}_3$ -type crystal structure with space group  $Pnma$ . It transforms into a corrugated layered  $\text{CaIrO}_3$ -type post-perovskite (pPv) structure at room temperature at 9 GPa [10]. A second structural phase transition occurs at 20 GPa from pPv-to-ppPv with the  $\text{Sb}_2\text{S}_3$ -type crystal structure [11]. The remarkable structural flexibility of  $\text{NaFeF}_3$  has made it an interesting candidate for studies and simulations of extreme environments, includ-

ing the Earth's interior and exoplanets [12].

The electronic configuration of the  $\text{Fe}^{2+}$  ions in  $\text{NaFeF}_3$  is high-spin (HS)  $t_{2g}^4 e_g^2$ . They follow the spin-only model with  $S = 2$  and a theoretical paramagnetic moment of  $\mu_{eff} = 4.90\mu_B$ , which is influenced by orbital contributions and usually leads to slightly higher  $\mu_{eff}$ .

$\text{Fe}^{2+}$  is air sensitive and oxidizes easily to  $\text{Fe}^{3+}$ . Controlling the anaerobic chemistry of  $\text{Fe}^{2+}$  ions is a prerequisite for synthesis of single phase  $\text{NaFeF}_3$ . We have previously utilized a solid state synthesis under inert conditions [10], yielding a sample with < 0.5 % Fe metal impurity. Impurities, either from an incomplete solid state reaction or from the iron reactor, may introduce inaccuracy to magnetometric studies and disguise the intrinsic magnetic behavior of  $\text{NaFeF}_3$ . Indeed, to the best of our knowledge there are no neutron powder diffraction (NPD) studies on the magnetic ordering in  $\text{NaFeF}_3$ , probably because the air sensitivity of  $\text{Fe}^{2+}$  makes it very difficult to produce sample volumes sufficient for NPD experiments by conventional solid state methods.

In this article we describe a wet-chemistry synthesis method for  $\text{NaFeF}_3$ , which produces iron-free material in substantial volumes. Using the high purity  $\text{NaFeF}_3$  samples, we study the intrinsic magnetic properties of the compound. Further, the magnetic structure is precisely described based on neutron powder diffraction data.

## II. EXPERIMENTAL

### A. Synthesis of NaFeF<sub>3</sub>

NaFeF<sub>3</sub> was synthesised on a Schlenk-line equipped with flexible hoses. Two polycarbonate vials of 85 and 200 ml volume (denoted A and B respectively) were used for the reaction. Vial A was filled with 2 g of Fe ( $\sim 0.035$  g mol<sup>-1</sup>, 99.999 % pure) and vial B with 0.08 mol ( $\sim 3.35$  g) NaF. The vials were closed tightly with silicone rubber septa, connected through the hoses to the Schlenk-line and thoroughly flushed with Ar. The Ar flow was maintained throughout the reaction to ensure inert conditions. A needle was placed in each septum to vent the excess gas from the vials. 10 mL of HCl (37 %) and 20 mL H<sub>2</sub>O were degassed, mixed and added to vial A. 20 mL of degassed H<sub>2</sub>O was carefully injected (using a syringe first evacuated and flushed with Ar) to the NaF in vial B. Both vials were placed in an oil-bath under constant Ar flow at 90 °C until the oxidation of Fe metal to FeCl<sub>2</sub> was completed. The FeCl<sub>2</sub> solution from vial A was then quickly transferred to vial B with an Ar flushed syringe. The contents of vial B were stirred constantly during injection to mix the two solutions. Thereafter, vial B was cooled to 80 °C and the contents stirred for 30 to 60 minutes. NaFeF<sub>3</sub> appeared as a beige precipitate. The product was washed repeatedly with degassed water and MeOH under flowing Ar, with decanting the liquid after each washing. Finally the solid product was removed from the vial, filtered, washed thoroughly with degassed MeOH, and dried under vacuum overnight before storing in the Ar-atmosphere of a glove box. Phase purity was confirmed by powder x-ray diffraction (PXRD) and magnetometry.

### B. Powder X-ray diffraction

PXRD data for NaFeF<sub>3</sub> were collected at the Norwegian National Resource Centre for X-ray Diffraction, Scattering and Imaging (RECX) on a Bruker D8 Advance diffractometer in capillary mode using CuK<sub>α1</sub> radiation (1.540598) selected by a Ge(111) focusing monochromator, and a LynxEye XE detector system.

### C. Magnetic characterization

Magnetometry experiments were performed with a 9T Physical Property Measurement System (PPMS, Quantum Design) on 48 mg of polycrystalline powder. Temperature dependent DC magnetic susceptibility  $\chi(T)$  measurements were conducted between 2 and 300 K for zero field cooled samples, followed by studies at field cooled conditions (ZFC and FC, respectively). The magnetic susceptibility is calculated by  $\chi = M/H$  where  $M$  is the magnetization, given in emu.mol<sup>-1</sup>Oe<sup>-1</sup> and  $H$  the

magnetic field (10 kOe). Isothermal field dependent measurements  $M(H)$  were collected at 2K, likewise half-loop isothermal measurements at 70, 120 and 300 K, all up to 90 kOe. AC measurements were carried out with frequencies ranging from 100 Hz to 10 kHz with a 10 Oe field.

### D. Neutron Powder Diffraction

NPD data for NaFeF<sub>3</sub> was measured on the WISH instrument at the ISIS pulsed neutron and muon source (UK) [13]. Diffraction patterns were collected between 2 and 297 K, and the data was reduced with the Mantid software [14]. Data from the four highest resolution detector banks were used, as the lowest resolution bank did not contain any unique information. NPD was collected at selected temperatures below and above  $T_N$ .

The magnetic refinements were carried out in the magnetic space group  $Pn'ma'$ , which allows non-zero values for  $M_x$ ,  $M_y$  and  $M_z$ , in the Jana2006 software [15]. The background (5 term Legendre polynomials), peak-shape, atomic positions (according to symmetry restrictions), isotropic thermal displacement parameters for each element type, lattice parameters and scale parameters were refined. The derived values for  $M_x$  and  $M_z$  are given in Table III.

## III. RESULTS

### A. Synthesis procedure and crystal structure

Fluoroperovskites are typically prepared by solid-state reactions and may contain magnetic impurities that make them appear as weak ferromagnets, both below and above the Néel temperature, as e.g.  $\alpha$ -Fe impurities in NaFeF<sub>3</sub> [10]. The air-sensitive chemistry of fluoroperovskites is demanding. We currently benefit from a new wet-chemical method that bypass the challenges of conventional solid-state reactions by always working under inert conditions on a Schlenk line. This wet-chemistry approach is ideal for synthesis of air-sensitive fluorides, as recently shown for the extremely air-sensitive Cr<sup>2+</sup> [16]. NaFeF<sub>3</sub> is currently prepared by means of this wet-chemical method, and high purity was confirmed by XRD and NPD.

NaFeF<sub>3</sub> adopts the distorted orthorhombic GdFeO<sub>3</sub> perovskite structure with space group  $Pnma$  and Glazer tilt  $a^-b^+a^-$ , Figure 1. The relation to the ideal cubic perovskite is given by  $a \approx c \approx \sqrt{2}a_c$  and  $b \approx 2a_c$  where  $a_c$  is the lattice parameter of the cubic perovskite. A weak Jahn-Teller distortion is present in the system originating from the high-spin  $d^6$  electron configuration of Fe<sup>2+</sup>. The consequence of the weak Jahn-Teller effect is slight differences in the bond lengths; the Fe-F1 bonds adopt a medium length (2.0744(3) Å), while Fe-F2 forms two short and two long bonds (2.0564(6) Å and

2.0795(6) Å respectively), Figure 1. Bond length values are from NPD at 297 K, see below.

### B. Magnetic properties

Variable temperature DC magnetization measurements were carried out on a polycrystalline sample between 2 and 300 K under a 10 kOe field (Figure 2). The data are consistent with long-range antiferromagnetic ordering. A sharp decrease in the molar magnetic susceptibility is associated with a Néel transition at 90 K. From the inverse susceptibility  $\chi^{-1}$  curve in the paramagnetic region (100 to 300 K), we calculate a paramagnetic moment of  $\mu_{eff} = 5.58 \mu_B$ . This is in good agreement with typically observed values for  $\text{Fe}^{2+}$  (5.0-5.6  $\mu_B$ ). From the Curie-Weiss fit, we extract a Weiss-temperature of  $\theta = -124$  K (data measured in a field of 10 kOe), confirming the dominating antiferromagnetic nature of  $\text{NaFeF}_3$ .

We note a significant difference between the FC and ZFC curves at low temperatures, as well as a minor hysteresis. This might indicate a transition to a spin-glass like state at low temperatures. However, AC magnetization measurements (Figure 3a) in a 10 Oe field show no variations of the Néel temperature versus frequency for  $\chi'$ , refuting this hypothesis.

Appearance of magnetic hysteresis may be explained by the presence of a small ferromagnetic moment originating from spin canting, resulting in weak ferromagnetism. For a purely antiferromagnetic transition, the imaginary component  $\chi''$  is expected to be zero in AC measurements [17]. In fact, for  $\chi''$  (Figure 3b) we observe a strong peak for an AC field of 10 kHz. The peak is less pronounced for 1 kHz AC field, while only noise is observed for 100 Hz AC field. The peak starts to increase in intensity at the Néel temperature, indicating that it is associated with the magnetic transition in  $\text{NaFeF}_3$ , and that we can excluded effects caused by an impurity, such as e.g.  $\alpha$ -Fe. It is therefore evident that spin-canting results in weak ferromagnetism in  $\text{NaFeF}_3$ , inherent to the compound. We note that the ferromagnetism is very weak and based on DC (Figure 2) and AC (Figure 3) magnetometry, it should be very close to zero in the absent of a magnetic field. The maximum of the peak is at  $\sim 32$  K, indicating that the spin-canting is further developing below the Néel temperature.

Isothermal field dependent magnetic measurements above the Néel temperature ( $T_N = 90$  K) at 120 and 300 K show a linear behaviour, associated with a paramagnetic state (Figure 4). The low magnetization observed at 90 kOe (0.25  $\mu_B/\text{Fe}$  at 2 K) confirms the dominating antiferromagnetic behavior of the system. However, below the Néel temperature, a slight hysteresis is observed. The hysteresis is clear at 2 K (inset in Figure 4), while it is less prominent at 70 K. The presence of hysteresis below  $T_N$  supports that weak ferromagnetism is intrinsic to the compound.

### C. Neutron diffraction and magnetic structure

Neutron diffraction was carried out between 2 and 297 K to investigate possible ordering of  $\text{Fe}^{2+}$  magnetic moments. At 2 K, strong additional reflections from long-range magnetic ordering are evident, e.g. two strong reflections at 4.49 and 4.58 Å and one weaker reflection at 7.89 Å (Figure 5 and Figure 10). These reflections were indexed according to the unit cell of the crystal structure of  $\text{NaFeF}_3$ , and corresponds to a  $\Gamma$ -point magnetic propagation vector  $k = (0,0,0)$ . However, several of the observed magnetic reflections break the symmetry extinctions of space group  $Pnma$ . We hence evaluated the possible magnetic structures for the  $\Gamma$ -point representations (Table I) by Rietveld refinements against NPD at 2 K, and we found  $\Gamma_4^+$  to precisely describe the magnetic ordering. This corresponds to the magnetic space group  $Pn'ma'$  (Figure 6).

TABLE I. Basis functions of the one-dimensional  $\Gamma$ -point irreducible representations found by decomposition of the magnetic representation for the iron site in  $\text{NaFeF}_3$ . The + and - symbols denote the relative sign of the magnetic moment along  $x$ ,  $y$ , and  $z$  on the respective site.

Coordinate			$\Gamma_1^+$			$\Gamma_2^+$			$\Gamma_3^+$			$\Gamma_4^+$		
$x$	$y$	$z$	$x$	$y$	$z$	$x$	$y$	$z$	$x$	$y$	$z$	$x$	$y$	$z$
0.0	0.0	0.5	+	+	+	+	+	+	+	+	+	+	+	+
0.0	0.5	0.5	-	+	-	+	-	+	+	-	+	-	+	-
0.5	0.5	0.0	+	-	-	-	+	+	+	-	-	-	+	+
0.5	0.0	0.0	-	-	+	-	-	+	+	+	-	+	+	-

The magnetic ordering of  $\Gamma_4^+$  can be described as  $A_x$  antiferromagnetic ordering along [001],  $F_y$  ferromagnetic ordering along [010] and  $G_z$  antiferromagnetic ordering along [001], corresponding to the refined parameters  $M_x$ ,  $M_y$  and  $M_z$  respectively (Table I). In our magnetic Rietveld refinements (Table II), we find a large value for the  $G_z$  component ( $M_z$ ) and a small value for the  $A_x$  component ( $M_x$ ). When performing Rietveld refinements of the ferromagnetic  $F_y$  component, a value of  $M_y = 0.75(3) \mu_B$  is obtained for the 2 K NPD data. However, since  $F_y$ -scattering coincides with nuclear peak positions, such quite small values of  $M_y$  yield very minor changes to the calculated diffraction pattern and agreement factors. Furthermore, these are strong correlations with other parameters of the refinements, e.g. the thermal displacement parameter of Fe. The ZFC magnetization measurement furthermore suggests that the ferromagnetic moment should almost absent at low temperatures without a magnetic field. As a consequence, the NPD data cannot be used to claim the existence of a  $F_y$  component. Hence,  $M_y$  was fixed to zero during the final refinements.

Complete structural details obtained from the Rietveld refinements of NPD data is given in Table II and Table III. The refined model has a dominating  $G_z$ -type antiferromagnetic structure with moments aligned parallel

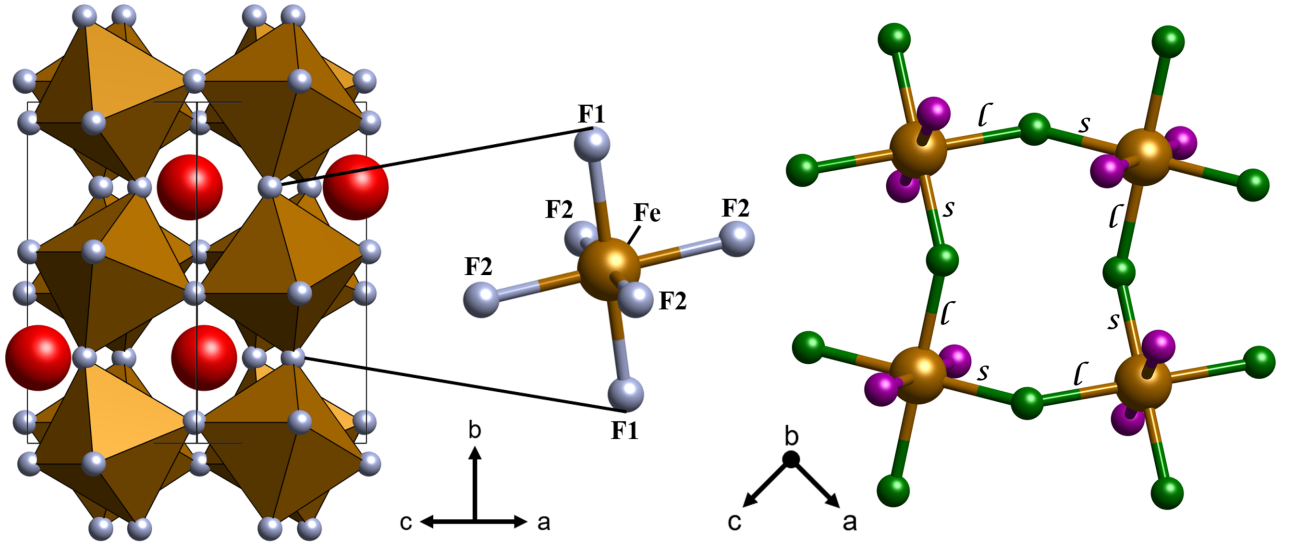


FIG. 1. Crystal structure of the orthorhombic perovskite  $\text{NaFeF}_3$  ( $Pnma$ ). Left: Illustration of the corner-connected octahedra of  $\text{FeF}_6$  with Glazer tilt  $a^-b^+a^-$ . Sodium, iron and fluorine atoms are shown in red, orange and gray, respectively. Right: Illustration of the  $ac$ -plane, where ordered short and long Fe-F2 bonds are formed by the weak Jahn-Teller effect. The short and long Fe-F2 bonds are marked  $s$  and  $l$  respectively, while medium Fe-F1 bonds are out-of-plane. Fe, F1 and F2 are shown in orange, purple and green, respectively.

TABLE II. Atomic coordinates of  $\text{NaFeF}_3$  from Rietveld refinement of NPD at 2 K. The refinement was performed in magnetic space group  $Pn'ma'$  with lattice parameters of  $a = 5.62571(11)$  Å,  $b = 7.87673(15)$  Å and  $c = 5.45623(10)$  Å, and magnetic parameters  $M_x = 0.422(11)$   $\mu_B$ ,  $M_y = 0$   $\mu_B$  and  $M_z = 4.221(4)$   $\mu_B$ , yielding a total ordered magnetic moment of  $M = 4.246(11)$   $\mu_B$ .

Site	Multiplicity	$x$	$y$	$z$	Occ	$U_{iso}$ (Å <sup>2</sup> )
Na	4	0.0544(2)	0.25	0.9826(3)	1	0.0175(4)
Fe	4	0.5	0	0	1	0.00438(17)
F1	4	0.45061(16)	0.25	0.11401(16)	1	0.0105(3)
F2	8	0.29707(11)	0.06114(8)	0.68918(11)	1	0.0096(2)

to [001]. There are weak indications for a small canting parallel to [100] as given by the  $A_x$  component (Figure 6). The magnetic moments are antiferromagnetically oriented with respect to their nearest neighbors along [010], [101] and  $[\bar{1}01]$ . Neighboring spins are aligned close to the equatorial plane of the octahedra (defined by the four F2 atoms, Figure 1) in the crystallographic (010)-plane.

At 2 K the Rietveld refinements give an ordered magnetic moment of  $4.246(11)$   $\mu_B$ , slightly lower than the theoretical spin-only value for  $\text{Fe}^{2+}$  of  $4.90$   $\mu_B$ . The value is in good agreement with that of  $\text{Fe}^{2+}$  in  $\text{KFeF}_3$ , which is  $4.42$   $\mu_B$  [21]. The slightly lower value than the spin-only value can be accounted for by a slight hybridization between iron and fluorine, effectively reducing the number of magnetically ordered electrons. A very weak additional ferromagnetic component will not change this picture, but should not be neglected, see below.

The refinements (and magnetic peak intensities) show

that the ordered magnetic moment decreases upon heating from 2 K. This is evidenced in the refined values for  $M_x$  and  $M_z$  (Figure 7a). The magnetic reflection in NPD disappears at 95 K, which is in compliance with the Néel temperature found by magnetometry.

We note the presence of a strong magnetostructural coupling in  $\text{NaFeF}_3$ , evidenced by major changes in the lattice parameters at the Néel ordering temperature (Figure 7b and c). At the transition, we observe a rather smooth contraction of the unit cell volume, however, this is an average of a contraction of the  $a$ -axis in contrast to expansion of the  $b$ - and  $c$ -axis.

Already at 120 K, well above the ordering temperature, we observe a change in temperature dependence for the  $b$ -axis (Figure 7). Actually, by evaluating the difference intensity plot between NPD patterns at 95 and 120 K (close to, and above the magnetic ordering temperature respectively), we observe a broad peak at around  $4.8$  Å (Figure 8), which corresponds to the position of the

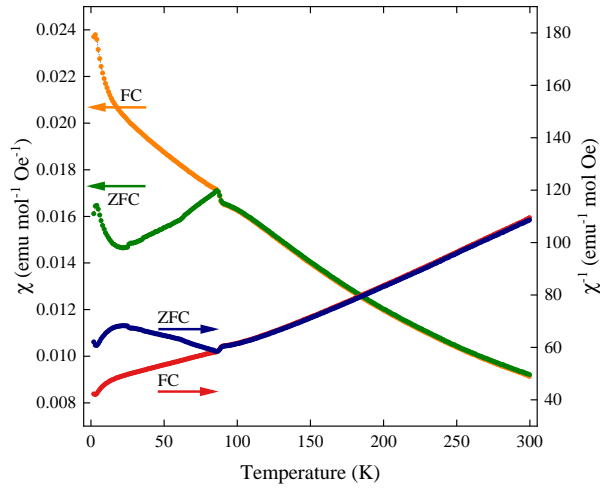


FIG. 2. Temperature dependency of the magnetic susceptibility  $\chi(T)$  at  $H = 10$  kOe measured in ZFC-FC mode (left axis) and inverse  $\chi^{-1}$  (right axis).

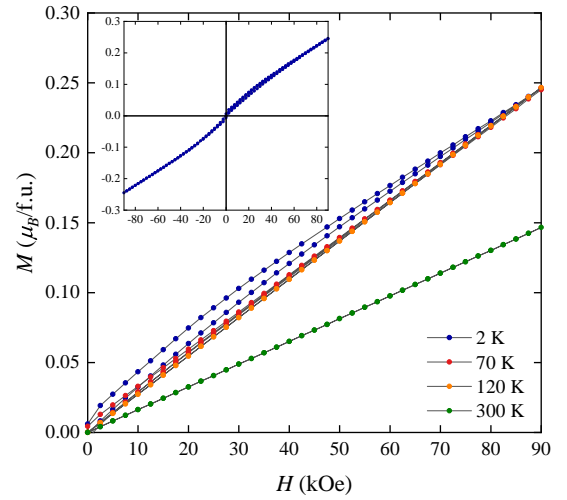


FIG. 4. Isothermal  $M$  versus  $H$  curves with an applied field  $0 \text{ T} \rightarrow 9 \text{ T} \rightarrow 0 \text{ T}$  recorded at 2, 70, 120 and 300 K. Insert:  $M$  versus  $H$  curve at 2 K to show the full symmetry.

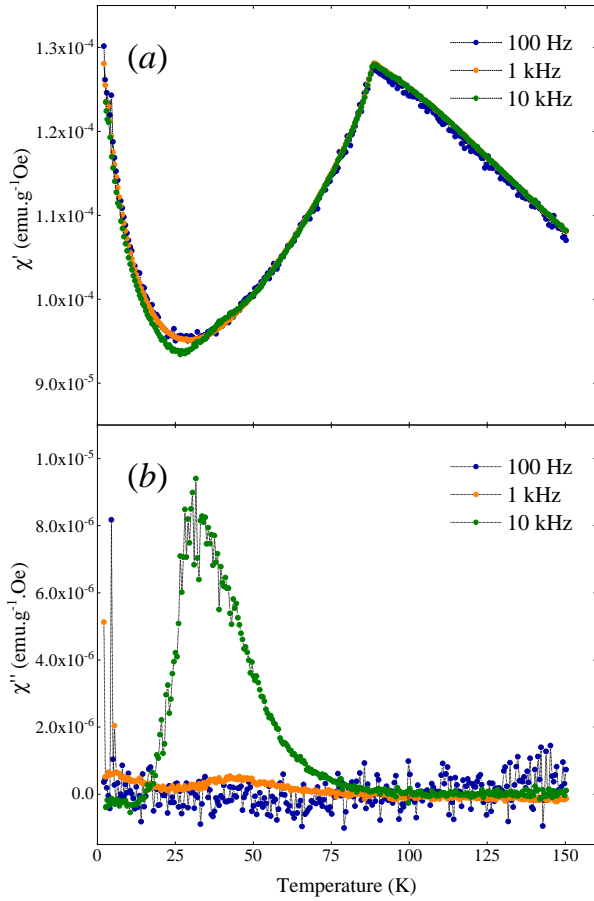


FIG. 3. Temperature dependence of the (a) real ( $\chi'$ ) and (b) imaginary ( $\chi''$ ) part of the AC magnetic susceptibility at different frequencies (100 Hz, 1 kHz and 10 kHz).

(011) and (110) magnetic Bragg reflections in the ordered

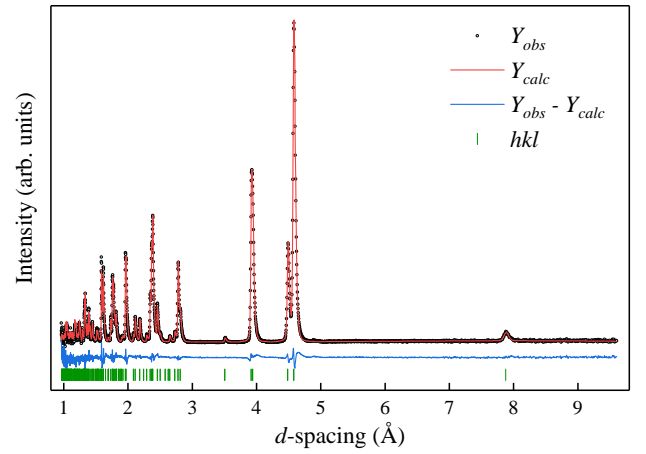


FIG. 5. Measured, calculated and difference curve from Rietveld refinement of the magnetic structure of  $\text{NaFeF}_3$  at 2 K for the second detector bank. The green ticks indicate reflections allowed by the magnetic symmetry (space group  $Pn'ma'$ ).

phase. The broad peak at  $4.8 \text{ \AA}$  is thus interpreted as originating from the existence of short-range magnetic ordering just above the Néel temperature.  $\text{Fe}^{2+}$  is reported to display magnetostrictive behavior and diffuse scattering above  $T_N$  in  $\text{Rb}_2\text{FeF}_4$ , and we note that the diffuse scattering for  $\text{NaFeF}_3$  above  $T_N$  also coincides with a tensile effect on the lattice [18].

As discussed above, due to a weak Jahn-Teller distortion,  $\text{NaFeF}_3$  adopts short, medium and long Fe-F bonds, Figure 1. Considering the variation of the Fe-F bond length between 2 and 297 K in the NPD experiment, we observe a clear trend: The bond lengths tend towards receiving identical values when temperature approaches 297 K (Figure 9). In the cubic perovskite  $\text{KFeF}_3$ , the

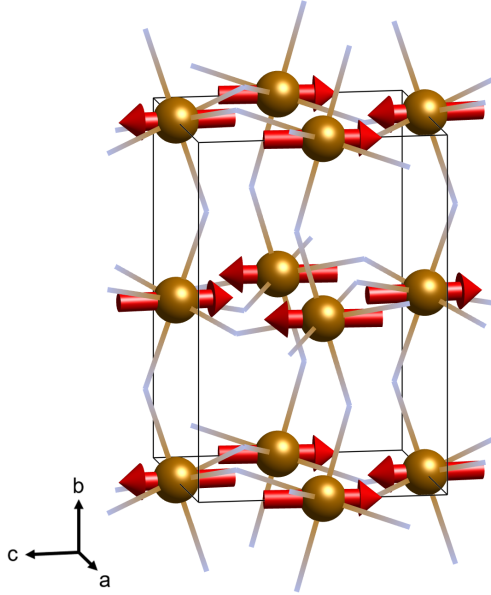


FIG. 6. Magnetic structure of the  $\text{NaFeF}_3$  with magnetic space group  $Pn'ma'$ . The magnetic moments of the iron atoms are antiferromagnetically ordered relative to their nearest neighbors, yielding G-type antiferromagnetism. Iron atoms are shown in orange and the bonds to fluorine as pale grey lines. Sodium atoms are removed for clarity.

Fe-F bond lengths adopts a value of  $2.06 \text{ \AA}$ , which ought to be a value expected also for the Fe-F bond lengths in  $\text{NaFeF}_3$  [19]. On this basis it is tempting to suggest that  $\text{NaFeF}_3$  may undergo transitions to higher symmetric structures at elevated temperatures [10, 11]. This is beyond the scope of the present work.

#### IV. DISCUSSION

We highlight that our new wet chemical synthesis protocol has allowed preparation of  $\text{NaFeF}_3$  of very high purity which is a prerequisite for clarification of intrinsic properties. Importantly, we compared ZFC - FC magnetic behaviour of phase pure samples with reported data for samples made by a conventional solid-state method [10]. For  $\text{NaFeF}_3$  prepared by solid-state methods, iron impurities easily outweigh the weak antiferromagnetic or paramagnetic signal, resulting in overestimated magnetization values. This is mirrored by a measured ferromagnetic behaviour at 300 K [10], which is not intrinsic to pure  $\text{NaFeF}_3$  prepared by our wet-chemical method. Note, that the very weak ferromagnetism observed in AC susceptibility below the Néel temperature of our phase pure  $\text{NaFeF}_3$  samples is intrinsic, but with value close to zero.

Although NPD cannot unambiguously conclude on the possible existence of a symmetry allowed ferromagnetic component along  $[010]$  ( $F_y$ ) according to the magnetic space group  $Pn'ma'$ , this is clearly indicated by a strong

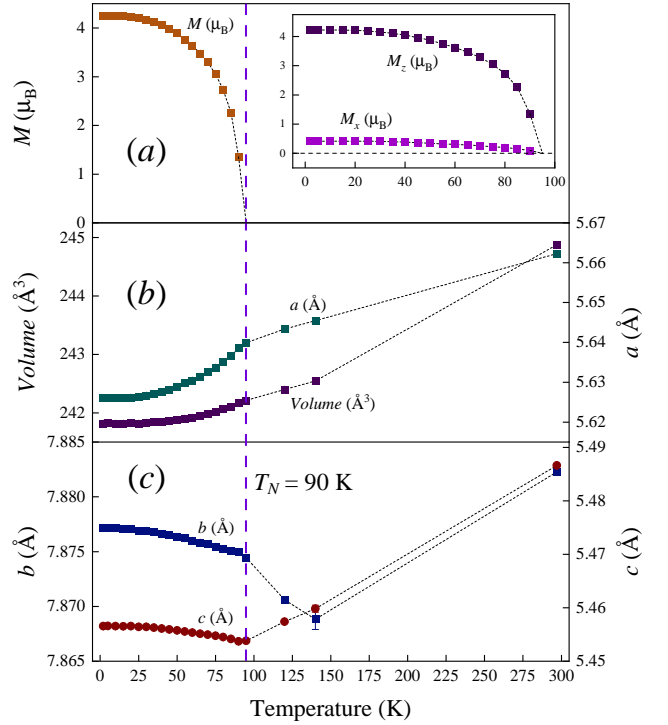


FIG. 7. Temperature dependence of structural parameters derived from Rietveld refinements of NPD; (a) the total magnetic moment, the inset show the  $M_x$  and  $M_z$  components, (b) lattice parameter  $a$  and cell volume, and (c) lattice parameter  $b$  and  $c$ . The Néel temperature of 90 K is indicated by the purple dashed line.

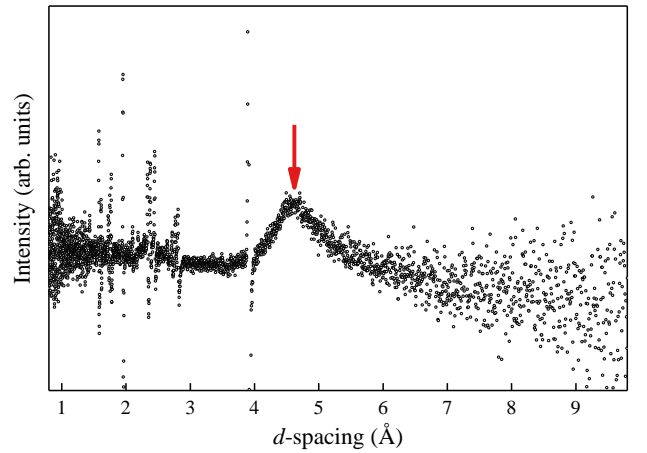


FIG. 8. Plot of the difference between NPD patterns at 95 and 120 K measured on the low resolution detector bank. A broad peak around  $4.8 \text{ \AA}$  is marked by a red arrow, which corresponds to the (011)- and (110)-magnetic Bragg reflections and indicates short-range magnetic order appearing at 95 K.

peak in the imaginary component  $\chi''$  of the AC susceptibility. Considering the magnetic F - Fe - F interactions of  $\text{NaFeF}_3$  in light of the Goodenough-Kanamori-Anderson

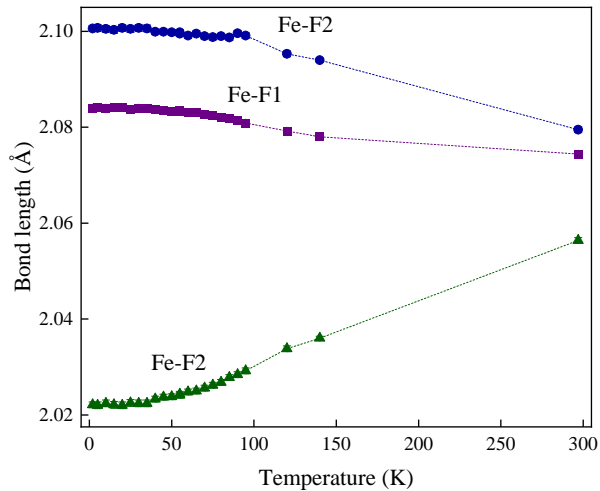


FIG. 9. Variation of the Fe-F bond lengths derived from Rietveld refinements of NPD between 2 and 297 K. Uncertainties are smaller than the symbol size.

(GKA) rules, antiferromagnetism is expected [20]. Furthermore, a linear G-type magnetic structure was predicted by DFT for  $\text{NaFeF}_3$  [10], also with moments arranged along [001] ( $G_z$ -type). However, our Rietveld analysis considered an additional weak  $A_x$ -component, which implies canting of the antiferromagnetism. The latter component is close to the detection limit of the analysis.

G-type magnetic ordering is observed in several other fluoroperovskites, e.g.  $\text{KMfF}_3$  ( $M = \text{Mn, Fe, Co, and Ni}$ ) [21]. However, due to the small sodium cation and the weakly Jahn-Teller active  $\text{Fe}^{2+}$ , the structure of  $\text{NaFeF}_3$  is significantly distorted and the F-Fe-F bond angles deviate from  $180^\circ$ . As a consequence, the interactions may deviate from the GKA rules.

Correspondingly, one must consider other magnetic interactions as origin to the weak ferromagnetism. For compounds with  $d^6$  electron configuration, Jahn-Teller, as well as spin-orbit interaction mechanism, will contribute to stabilization of the system [22]. If spin-orbit

coupling is present in  $\text{NaFeF}_3$ , Dzyaloshinskii-Moriya interactions may occur. Such interactions give rise to ferromagnetic exchange and may thus be the origin of weak ferromagnetism in  $\text{NaFeF}_3$  [23, 24].

## V. CONCLUSION

In summary we have developed a wet-chemical synthesis protocol that allow preparation of  $\text{NaFeF}_3$  in large quantities and of high purity. As a consequence we have been able to investigate the intrinsic magnetic properties of  $\text{NaFeF}_3$  without potential additional magnetic contributions from impurities like  $\alpha\text{-Fe}$  that will interfere with the analysis. Magnetic susceptibility and powder neutron diffraction analysis shows that  $\text{NaFeF}_3$  has a Néel temperature of 90 K. AC magnetometry clearly show the presence of weak ferromagnetism below the ordering temperature, supported by field dependent DC measurements. Neutron diffraction data describe the compound as a weakly canted  $G_z$ -type antiferromagnet with a minor  $A_x$ -component allowed by symmetry. The magnetic space group opens for a  $F_y$  component, however, this is almost absent at zero-field and is too weak to be proven the current analysis. The temperature variation of the Fe-F bonds suggest a possible structural phase transition to a higher symmetric structure above 300 K.

## VI. ACKNOWLEDGEMENTS

We thank Serena Margadonna (Swansea University, Swansea, UK) for providing project support via the Research Council of Norway project 214260. This work was partially performed within the RIDSEM-project, financed by the Research Council of Norway (Project No. 272253). The U.K. Science and Technology Facilities Council (STFC) is thanked for allocating beamtime at the ISIS Facility. We also thank Pascal Manuel for help during the NPD experiment, and Asbjørn Slagtern Fjellvåg and Vincent Hardy for discussions regarding magnetic properties.

- 
- [1] M. Leblanc, V. Maisonneuve and A. Tressaud *Chem. Rev.*, **115**, 1191–1254, 2015
- [2] A. Tressaud *J. Fluorine Chem.*, **132**, 1191–1254, 2011
- [3] R.M. Dubrovin, L.N. Alyabyeva, N.V. Siverin, B.P. Gorskunov, N.N. Novikova, K.N. Boldyrev, and R.V. Pisarev *Phys. Rev. B*, **101**, 180403, 2020
- [4] R.M. Dubrovin, S.A. Kizhaev, P.P. Syrnikov, J.-Y. Gesland, and R.V. Pisarev *Phys. Rev. B*, **98**, 060403, 2018
- [5] H. Béa, M. Gajek, M. Bibes and A. Barthélémy *J. Phys. Condens. Mat.*, **20**, 434221, 2008
- [6] I. Žutić, J. Fabian and S.D. Sarma *Rev. Mod. Phys.*, **76**, 323, 2004
- [7] A. Kitajou, H. Komatsu, K. Chihara, I.D. Gocheva, S. Okada and J. Yamaki *J. Power Sources*, **198**, 389–392, 2012.
- [8] Y. Yamada, T. Doi, I. Tanaka, S. Okada and J. Yamaki *J. Power Sources*, **196**, 4837–4841, 2011.
- [9] K.V. Kravchuk, T. Žiđ, M. Worle, M.V. Kovalenko and M.I. Bodnarchuk *Chem. Mater*, **30**, 1825–1829, 2018.
- [10] F.L.M. Bernal, K.V. Yusenko, J. Sottmann, C. Drathen, J. Guignard, O.M. Iøvvik, W.A. Chrichton and S. Margadonna *Inorg. Chem*, **53**, 12205–12214, 2014.
- [11] W.A. Chrichton, F.L.M. Bernal, J. Guignard, M. Hanfland and S. Margadonna *Mineralogical Magazine*, **80**, 659–674, 2016.

- [12] J.M. De Teresa, M.R. Ibarra, P. Algarabel, L. Morellon, B. Garca-Landa, C. Marquina, C. Ritter, A. Maignan, C. Martin, B. Raveau, A. Kurbakov, and V. Trounov *Phys. Rev. B*, **65**, 100403, 2002.
- [13] L.C. Chapon, P. Manuel. *Neutron News*, **22**, 22, 2011
- [14] O. Arnold, J.C. Bilheux, J.M. Borreguero, A. Buts, S.I. Campbell, L. Chapon, M. Doucet, N. Draper, R. Ferraz Leal, M.A. Gigg, V.E. Lynch, A. Markvardsen, D.J. Mikkelson, R.L. Mikkelson, R. Miller, K. Palmen, P. Parker, G. Passos, T.G. Perring, P.F. Peterson, S. Ren, M.A. Reuter, A.T. Savici, J.W. Taylor, R.J. Taylor, R. Tolchenov, W. Zhou and J. Zikovsky *Nucl. Instrum. Methods Phys. Res. A*, **764**, 156, 2014.
- [15] V. Petříček, M. Dušek and L. Palatinus *Z.Kristallogr. Cryst. Mater*, **229**, 345, 2014
- [16] F.L.M. Bernal, J. Sottmann, D.S. Wragg, H. Fjellvåg, Ø.S. Fjellvåg, C. Drathen, W.A. Ślawiński, and O.M. Løvvik *Phys. Rev. Materials*, **4**, 054412, 2020
- [17] A. Szytuła, M. Bałanda, B. Penc and M. Hofmann *J. Phys.: Condens. Matter*, **12**, 7455–7462, 2000
- [18] R.J. Birgeneau, H.J. Guggenheim and G. Shirane *Phys. Rev. B*, **1**, 2211, 1970.
- [19] R.J. Birgeneau, H.J. Guggenheim and G. Shirane *Acta Cryst. B*, **39**, 561–564, 1983.
- [20] J.B. Goodenough *Magnetism and the Chemical Bond*, R. E. Krieger Publishing Company, 1976
- [21] V. Scatturin, L. Corliss, N. Elliott and J. Hastings *Acta Cryst.*, **14**, 19–26, 1961
- [22] K.I. Kugel' and D.I. Khomskii *Sov. Phys. Usp.*, **25**, 231, 1982
- [23] I. Dzyaloshinsky *J. Phys. Chem. Solids*, **4**, 241–255, 1958
- [24] T. Moriya *Phys. Rev.*, **120**, 91, 1960



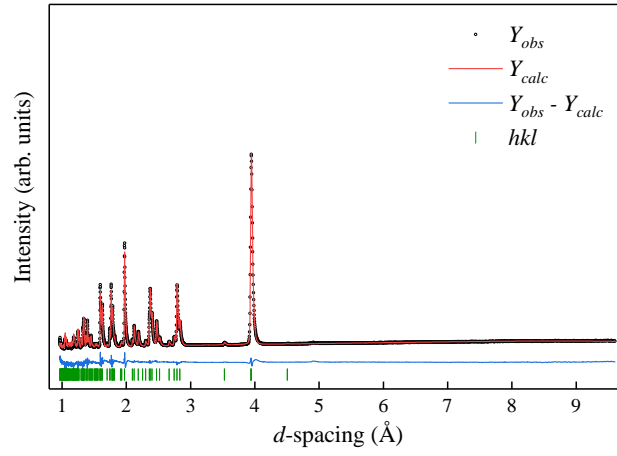


FIG. 10. Measured, calculated and difference curve from Rietveld refinement of the nuclear structure of  $\text{NaFeF}_3$  at 297 K for the second detector bank. The green ticks indicate reflections allowed by the space group ( $Pnma$ ).

TABLE III. Atomic coordinates and magnetic moments  $M_x$ ,  $M_y$  and  $M_z$  for Fe in  $\text{NaFeF}_3$  derived from Rietveld refinements of NPD data below  $T_N$ . The refinement was performed in magnetic space group  $Pn'ma'$ .

Temperature (K)	$x$	$y$	$z$	$M_x$	$M_y$	$M_z$
2	0.5	0	0	0.42(1)	0	4.224(4)
5	0.5	0	0	0.41(1)	0	4.223(4)
10	0.5	0	0	0.41(1)	0	4.223(4)
15	0.5	0	0	0.41(1)	0	4.223(4)
20	0.5	0	0	0.41(1)	0	4.210(4)
25	0.5	0	0	0.41(1)	0	4.189(4)
30	0.5	0	0	0.40(1)	0	4.153(4)
35	0.5	0	0	0.39(1)	0	4.108(4)
40	0.5	0	0	0.38(1)	0	4.048(4)
45	0.5	0	0	0.36(1)	0	3.964(4)
50	0.5	0	0	0.34(1)	0	3.875(4)
55	0.5	0	0	0.32(1)	0	3.743(3)
60	0.5	0	0	0.30(1)	0	3.624(3)
65	0.5	0	0	0.28(1)	0	3.468(3)
70	0.5	0	0	0.25(1)	0	3.288(3)
75	0.5	0	0	0.22(1)	0	3.045(3)
80	0.5	0	0	0.19(1)	0	2.733(3)
85	0.5	0	0	0.15(2)	0	2.256(3)
90	0.5	0	0	0.09(4)	0	1.354(4)